Full Paper

Propellants, Explosives, Pyrotechnics

DOI: 10.1002/prep.201200210

Multiscale Simulation on the Influence of Dimethyl Hydantoin on Mechanical Properties of GAP/RDX Propellants

Yanhua Lan,[a] Jinxian Zhai,*[b] Dinghua Li,[a] and Rongjie Yang[a]

Abstract: The influence of dimethyl hydantoin (DMH) on the mechanical properties of GAP/RDX propellant was studied by molecular dynamics (MD) and dissipative particle dynamics (DPD) simulation. The results showed that the binding energies ($E_{binding}$) between GAP and different surfaces of RDX were in the order of (010) > (001) > (100). Compared to GAP/RDX, GAP grafted with DMH (GAP-DMH) exhibits higher binding energies with RDX, and the sequence of $E_{binding}$ turns to (001) > (010) > (100). Radial distribution simulations demonstrated that GAP-DMH is more close to the surfaces of RDX, increasing the van der Waals energies between GAP-DMH and RDX. The stress and strain of GAP-DMH/RDX excel those of GAP/RDX. DPD simulations showed that GAP-DMH was able to restrain the agglomeration of RDX, to improve the dispersibility and to enlarge the contact surface with RDX, which also increased the mechanical properties of GAP/RDX propellant.

Keywords: GAP/RDX propellants · Multiscale simulation · Binding energy · Dispersibility · Mechanical properties

1 Introduction

Azido polymers have attracted research attention over the past two decades since azido-containing components are able to contribute to a high positive formation enthalpy. The hydroxyl terminated glycidyl azide polymer (GAP) (see Scheme 1) has become a research focus because of its high density, high oxygen balance, and low glass transition temperature [1, 2].

Cyclotrimethylene trinitramine (RDX), a cyclic trimer of methylenenitramine, is one of the most important crystalline energetic materials and is widely employed to improve the performances of propellants [3, 4]. Combining RDX and GAP is an important approach in the manufacturing of high-performance, low-signature propellants. Unfortunately, addition of RDX to GAP composite propellants always adversely affects the mechanical properties of the resulting propellant [5–9]. Nevertheless, the use of bonding agents offers an important approach for improving the mechanical properties of propellants [10–12].

Hydantoin compounds are recognized as a class of bonding agents and are widely used in RDX-based propellants to improve mechanical properties. Consaga [13] added bis(2-hydroxyethyl) dimethyl-hydantoin to HTPB composite propellants and found that there was a strong interaction between the binder HTPB and the filler RDX. Liu [14] considered that hydantoin bonding agents could interact with the $-NO_2$ groups of the RDX molecule and thereby improve the mechanical properties of HTPB/RDX/Al propellants. However, the application of hydantoin compounds in GAP composite propellants has only been scarcely reported.

Recently, molecular simulation has become a powerful tool in the field of materials research. In composite molecular systems, it is able to simulate microscopic and mesoscopic structures and characterize the interfacial behavior [15, 16]. For example, Li [17] studied the binding energy of GAP/RDX employing the COMPASS force field. The results indicated that the binding energies on different crystalline surfaces of RDX are different from each other. Gai [18] simulated mesophase formation in binary UHMWPE/ PP and ternary UHMWPE/PP/PEG blends by a dissipative particle dynamics (DPD) simulation method.

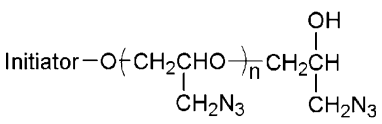

Scheme 1. Molecular structure of GAP.

[a] *Y. H. Lan, D. Li, R. J. Yang*
School of Material Science and Engineering
Beijing Institute of Technology
Haidian District, Beijing, P. R. China

[b] *J. X. Zhai*
School of Material Science and Engineering
Beijing Institute of Technology
5 South Zhongguancun Street
Haidian District, Beijing, P. R. China
**e-mail: zhjx@bit.edu.cn*

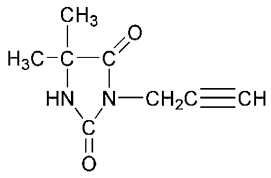

Scheme 2. Molecular structure of PDMH.

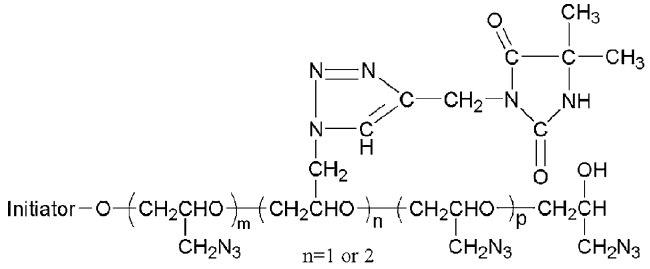

Scheme 3. Molecular structure of GAP-DMH.

In order to improve the mechanical properties of GAP/RDX propellants, we synthesized 3-propargyl-5,5-dimethyl hydantoin (PDMH, see Scheme 2), and prepared GAP grafted with dimethyl hydantoin (GAP-DMH, see Scheme 3) through a click chemistry reaction between the azido and alkyne functions. In the work presented herein, molecular dynamics (MD) simulation was used to simulate the binding energy, the radial distribution function between the polymers and RDX, and the mechanical properties of their composite propellants. Moreover, DPD was applied to simulate the mesoscopic morphologies of GAP composite propellants. The results showed that DMH grafted onto GAP could effectively improve the mechanical properties of GAP/RDX propellants.

2 Modeling and Simulation Method

2.1 Molecular Model Construction and Simulation Method

The models used in the simulation were constructed using materials studio package (MS 5.5). The structure of RDX used in the condensed phase simulations was taken from the experimental data [19]. RDX is a crystal belonging to the monoclinic space group of PBCA with four independent lattice parameters $a = 1.318$ nm, $b = 1.157$ nm, $c = 1.071$ nm, and $\alpha = \beta = \gamma = 90^\circ$, and its density is 1.816 g cm^{-3}. There are eight irreducible molecules in the unit cell (see Figure 1). To investigate the differences in the properties among the various crystalline surfaces, the cell was cleaved along three crystalline surfaces (100), (010), and (001), and periodic unit cells (3×2×1), (2×3×1) and (4×3×1) were determined to construct RDX simulation model.

The GAP amorphous cell contained two GAP chains. Each GAP chain consisting of 22 monomers was established to represent the real molecular chain. A GAP-DMH amorphous cell was established as follows. (1) Two GAP chains

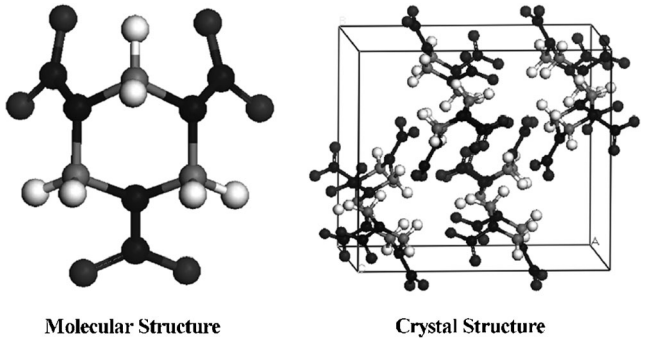

Figure 1. Molecular and crystal structures of RDX.

and three molecules of PDMH were mixed and allowed to be thermal equilibrium. (2) PDMH molecules were considered to react with the nearest azido group and generated GAP-DMH.

In contrast to the RDX crystal, the GAP and GAP-DMH polymer chains adopt amorphous conformations, and the amorphous arrangements having the lowest energies were adopted for the simulation. We then assembled molecular layer structures of GAP/RDX and GAP-DMH/RDX, layering the polymer chains on the different crystalline surfaces of RDX and retaining a 2 nm vacuum layer over the polymer layer.

Prior to the MD simulations, 5000 steps of energy minimization using the smart minimizer method were performed to relax all of the structures in the system. The relaxed structures were further subjected to five time annealing from 600 K to 300 K at 50 K intervals to overcome the local minimum energy barriers. At each annealing, 120 ps NVT MD simulation was performed. The conformation corresponding to minimum energy was extracted, and a 500 ps NVT ensemble MD simulation was carried out. A final 50 ps was used for analyzing solubility parameters of GAP, PDMH, and RDX, including binding energies, radial distribution function and the mechanical properties of polymer/RDX. Coulombic and van der Waals long-range nonbonding interactions were handled by the standard Ewald and atom-based summation methods, respectively. Nonbonding interactions, spline width, and buffer width were truncated at 0.95, 0.1, and 0.05 nm, respectively. The Andersen algorithm [20] was used for temperature control (thermostat), using a collision rate of 1.0, and the temperature was set at the ambient 298 K. COMPASS, which is able to accurately predict the structural, conformational, vibrational, and thermophysical properties for a broad range of compounds both in the isolation and condensed phases, was employed to simulate the GAP/RDX system [21–23].

Additionally, a radial distribution function $g(r)$ was used to characterize the probability of finding another atom at a certain distance from a specific atom in the GAP/RDX and GAP-DMH/RDX systems. The higher the value of $g(r)$, the greater the likelihood of finding an atom in the corresponding position. It is defined according to Equation (1).

$$g_{AB}(r)=\frac{1}{\rho_{AB}4\pi r^2}\frac{\sum_{i=1}^{\kappa}\sum_{j=1}^{N_{AB}}\Delta N_{AB}(r\rightarrow r+\Delta r)}{N_{AB}\times\kappa} \quad (1)$$

where N_{AB} is the total number of atoms of A and B in the system, κ is the number of time steps, Δr is the distance interval, ΔN_{AB} is the number of B (or A) atoms between r to $r+\Delta r$ around an A (or B) atom, ρ_{AB} is the bulk density [24].

2.2 Mesoscopic Modeling Construction and Simulation Method

In order to probe the microstructural morphologies of GAP/RDX composite propellants, the mass ratio of GAP to RDX was taken to be 3:7. The DPD program as implemented in the MS package was used to simulate the mesoscopic structure. In DPD approach, several molecules or repeat units, which has equivalent volume, are defined as a separated bead. To investigate the influence of DMH on the morphology, a PDMH segment was considered as a bead and the amounts of beads of polymer and RDX were determined according to the volume fraction of PDMH. The repulsion parameters used in the DPD simulation were obtained according to Equation (2) and Equation (3) [25].

$$a_{ij}=a_{ii}+3.27\,\chi_{ij} \quad (2)$$

$$\chi_{ij}=\frac{(\delta_1-\delta_2)^2\,V_{mon}}{RT} \quad (3)$$

Here, a is a repulsion parameter, χ is the Flory-Huggins parameter, V_{mon} is the average molar volume of monomer, R is the gas constant, 8.314 J·(mol·K)$^{-1}$, T is the equilibrium temperature, 298 K, and δ are the solubility parameters of GAP, RDX, and PDMH molecular, which were evaluated as 18.08, 27.48, and 25.82 (J·cm^{-3})$^{1/2}$, respectively, by MD simulation. According to references [26, 27] the a_{ii} values of GAP, RDX, and PDMH are 25.00, 25.00, and 5.00, respectively. And, the density and spring constant used in the simulation were set as 3.0 and 4.0, respectively. The grid dimensions were chosen as 30×30×30, and the mesoscale morphologies were portrayed in DPD length units using a grid spacing of 1.0. The maximum number of iterations per step was 0.05 and a total of 100 000 steps were carried out.

3 Results and Discussion

3.1 Binding Energy

Binding energy ($E_{binding}$) can reflect the interaction capacity of two components, which is defined as the negative value of the intermolecular interaction energy (E_{inter}). The $E_{binding}$ between the polymer and RDX was determined according to Equation (4).

$$E_{binding}=-E_{inter}=-(E_{total}-E_{polymer}-E_{RDX}) \quad (4)$$

where E_{total} is the total energy of the polymer/RDX system. E_{RDX} and $E_{polymer}$ are the energies of RDX and the polymer GAP or GAP-DMH, respectively.

Table 1 shows the energies evaluated by MD simulation and reported in the reference [17]. Comparing binding energies evaluated here with those reported in reference [17], it can be seen that the energy values of RDX [17] are almost as twice as the energy values presented herein. This is mainly resulted from the differences of the model constructed. In the model used here, a 2 nm vacuum layer was retained over the polymer layer, while in the reference [17], the model constructed had not retained vacuum layer, so that the energies of RDX were calculated twice (upper and bottom contact surfaces). As for the energies of E_{total} and $E_{polymer}$, there does not exist comparability due to the difference of degree of GAP polymerization (the degrees of GAP polymerization are 22 and 8 in this paper and reference [17], respectively). Though, it should be pointed out that the degree of GAP polymerization employed here is more closed to the real application situation.

From Table 1, it can also be seen that the $E_{binding}$ between the polymer and RDX simulated here is solely attributable to nonbonding energy (van der Waals energy and electrostatic energy). Moreover, the binding energies are mainly attributable to the E_{VDW}, while the $E_{electrostatic}$ only accounts for a small portion. For the GAP/RDX system, the highest

Table 1. Binding energies simulated and reported [kJ mol^{-1}].

Interface	E_{total}	$E_{polymer}$	E_{RDX}	$E_{binding}$	$E_{nonbond}$	$E_{nonbonding}$	
						E_{VDW}	$E_{electrostatic}$
GAP/RDX(001) [17]	−71968.26	1270.12	−71988.67	1249.71	–	–	–
GAP/RDX(010) [17]	−71768.38	1788.57	−71350.78	2206.13	–	–	–
GAP/RDX(100) [17]	−71726.42	1698.31	−71439.98	1984.75	–	–	–
GAP/RDX(001)	−33376.69	3245.47	−36529.33	92.82	92.82	67.91	24.91
GAP/RDX(010)	−30773.40	5710.11	−36241.09	242.42	242.42	183.62	58.80
GAP/RDX(100)	−30139.54	5728.17	−35783.08	84.63	84.67	57.50	27.17
GAP-DMH/RDX(001)	−34260.62	2938.78	−36705.52	493.92	493.92	352.93	140.95
GAP-DMH/RDX(010)	−32785.91	4034.23	−36552.94	267.25	267.25	203.28	63.97
GAP-DMH/RDX(100)	−31768.30	4137.21	−35772.37	133.14	133.14	92.95	40.15

binding energy exists on the (010) interface, and the $E_{binding}$ on the different interfaces rank in the order of (010) > (001) > (100).

In comparison with binding energies of GAP/RDX system, the highest binding energy exists on the (001) interface in GAP-DMH/RDX system, and the most significant change in binding energy also occurs on this interface. The $E_{binding}$ on different interfaces rank in the order of (001) > (010) > (100) in the GAP-DMH/RDX system. It should be noted that that all binding energies in GAP-DMH/RDX system are higher than those in GAP/RDX system. This indicates that DMH grafted onto GAP could simultaneously increase the electrostatic energy and van der Waals energy between GAP and RDX.

3.2 Radial Distribution Simulation

For conciseness, only the model structure of polymer/RDX (001) is shown in Figure 2. It can be seen that GAP on the (001) surface of RDX adopts a straight conformation, while GAP-DMH seems to adopt a collapsed conformation, exhibiting a larger contact surface and better permeability with the (001) surface of RDX.

Figure 3 shows the inter-g(r) dependence on radial distance r in the range of 0–2 nm. For the GAP/RDX system, the curve for GAP/RDX(010) is higher than that for GAP/RDX(001), which is in turn higher than that for GAP/RDX(100). The van der Waals force is operative when the distance between atoms is less than 0.5 nm, the strength of which is proportional to the number of particles [28]. Thus, it can be deduced that the van der Waals energy between GAP and RDX(010) is the highest, while that between GAP and RDX(100) is the lowest. In like manner, in the GAP-DMH/RDX system the van der Waals energy between GAP-DMH and RDX(001) is the highest, while that between GAP-DMH and RDX(100) is the lowest. These are

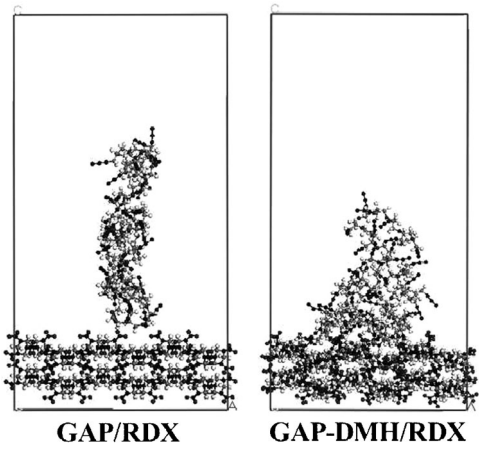

Figure 2. Molecular layer structures of the polymer on the (001) surface of RDX (upside: GAP or GAP-DMH; downside: RDX).

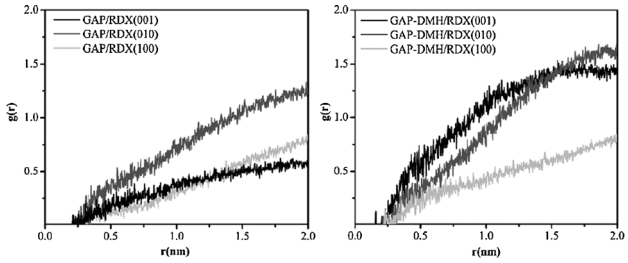

Figure 3. Radial distribution function g(*r*) between RDX and polymers.

is in good agreement with the results of the binding energy simulation (see Table 1).

Comparing Figure 2 and Figure 3, higher values of *g*(r) occur in the range of 0.2–2.0 nm in GAP-DMH/RDX. Because the difference between GAP-DMH/RDX and GAP/RDX stems from the dimethyl hydantoin structure appended onto the backbone of GAP, and dimethyl hydantoin has strong affinity towards RDX [29]. Those can be concluded that DMH grafted onto GAP increases the affinity between GAP and RDX and the approach between GAP-DMH and RDX also strengthens their van der Waals force, so the van der Waals energies in the GAP-DMH/RDX system would be higher than those in the GAP/RDX system, which are in accordance with the results of the energy simulation (See Table 1). Additionally, due to the more compact form of GAP-DMH on the RDX surface, this is beneficial to improve the strain of the GAP/RDX propellant. These suggest that DMH grafted onto GAP can help to improve the stress and the strain of the GAP/RDX propellant.

3.3 Mechanical Properties

Material stress and strain tensors are denoted by σ and ε, respectively. According to the reports in the reference [30], σ and ε are expressed as Equation (5) and Equation (6). They are applicable for materials exhibiting small deformations when subjected to external forces. Thus, the dependence of the stress on the strain for elastic materials can be written as Equation (7), where *C* is a 6×6 matrix [31].

$$\sigma = (\sigma_{11}, \sigma_{22}, \sigma_{33}, \sigma_{12}, \sigma_{23}, \sigma_{31})^T \quad (5)$$

$$\varepsilon = (\varepsilon_{11}, \varepsilon_{22}, \varepsilon_{33}, 2\varepsilon_{12}, 2\varepsilon_{23}, 2\varepsilon_{31})^T \quad (6)$$

$$\sigma_i = C_{ij}\ \varepsilon_j \quad (7)$$

C_{ij} (i, j = 1, 2,…,6) are the elements of the elastic symmetric matrix *C*, and up to a maximum of 21 constants are required to fully describe the stress-strain behavior of an arbitrary material [31]. The compliance matrix *S* is the inverse matrix of the elastic symmetric matrix *C*, i.e., $S = C^{-1}$.

The effective isotropic compliances in terms of single-crystal compliances averaged over all orientations can be

Table 2. The modeled mechanical properties of GAP/RDX and GAP-DMH/RDX.

	GAP/RDX			Average	GAP-DMH/RDX			Average
	(001)	(010)	(100)		(001)	(010)	(100)	
Bulk modulus *K* [GPa]	0.89	0.69	0.53	0.70	1.54	1.74	0.71	1.33
Shear modulus *G* [GPa]	0.52	0.42	0.33	0.42	0.74	1.00	0.45	0.73
Poisson's ratio ν	0.26	0.25	0.24	0.25	0.29	0.26	0.24	0.27
Tensile modulus *E* [GPa]	1.31	1.05	0.82	1.05	1.91	2.52	1.11	1.85
K/*G*	1.71	1.64	1.61	1.65	2.08	1.74	1.58	1.80

obtained by the Reuss average. Thus, the effective bulk moduli (*K*) and shear moduli (*G*) are given by Equation (8) and Equation (9), respectively, where the subscript R denotes the Reuss average. The isotropic linear elasticity *E* and Poisson's ratio ν can be obtained from Equation (10).

$$K_R = [S_{11} + S_{22} + S_{33} + 2(S_{12} + S_{23} + S_{31})]^{-1} \quad (8)$$

$$G_R = 5[4(S_{11} + S_{22} + S_{33}) - 4(S_{12} + S_{23} + S_{31}) + (S_{44} + S_{55} + S_{66})]^{-1} \quad (9)$$

$$E = 2G\ (1 + \nu) = 3K\ (1-2\nu) \quad (10)$$

The predicted effective isotropic mechanical properties are summarized in Table 2. As can be seen from Table 2, the *K*, *G*, and *E* for GAP/RDX system gradually increase from the surface (001) to (100). Different from the results above, the K gradually decreases from the surface (010) to (001) in reference [17], as may be aroused from the different molecular weight of GAP. In comparison with GAP/RDX, all of the bulk moduli, shear moduli and tensile moduli of GAP-DMH/RDX on the different interfaces of RDX are distinctly increased. Correspondingly, their averages also increase from 0.70, 0.42, and 1.05 GPa to 1.33, 0.73, and 1.85 GPa, respectively. Because the fracture strengths of materials are proportional to their bulk moduli *K* [29], GAP-DMH/RDX propellant should possess better mechanical strength.

The ratio of bulk moduli to shear moduli (*K*/*G*) can be used to evaluate the ductility of a material, and a high value of *K*/*G* is associated with ductility and low brittleness. In comparison with the GAP/RDX system, the value of *K*/*G* on the (100) surface is lower in the GAP-DMH/RDX system, but their average (1.80) is higher than that in the GAP/RDX system (1.65). This suggests that GAP-DMH/RDX system also possesses higher strain in comparison with GAP/RDX system. These results are consistent with the analysis of the radial distribution function.

3.4 Morphology Simulation

Besides the interface interaction between the binder and the solid fillers, the dispersibility of solid fillers also plays an important role in the mechanical properties of composite propellants. The better the dispersibility, the larger the contact area between the binder and the filler, and the more the mechanical properties could be helped to be improved. The mesoscale morphologies of polymers/RDX were simulated by DPD simulation, and values of the Flory-Huggins interaction parameter a_{ij} used in the DPD simulation are listed in Table 3. Figure 4 depicts the mesoscale morphologies of the GAP/RDX and GAP-DMH/RDX propellants.

Table 3. Interaction parameters (a_{ij}) in DPD simulation.

Interaction parameters	GAP	RDX	PDMH
GAP	25.00	36.42	33.16
RDX	36.42	5.00	25.46
PDMH	33.16	25.46	25.00

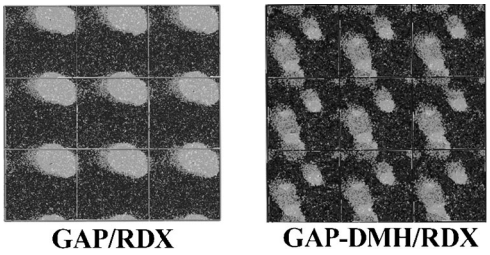

Figure 4. Morphologies of RDX in GAP/RDX and GAP-DMH/RDX. (dark: GAP or GAP-DMH; light: RDX).

It becomes obvious from Figure 4 that RDX forms larger agglomerates in the GAP/RDX system, while it forms smaller agglomerates in the GAP-DMH/RDX system. This indicates that in comparison to GAP, GAP-DMH can suppress the agglomeration of RDX particles, and improves the dispersibility of RDX. Thus it can be infered that GAP grafted with dimethyl hydantoin can be well coated on the surface of smaller particles, increases the effective contact areas with RDX, and helps to improve the mechanical properties of GAP/RDX propellants.

4 Conclusions

MD and DPD simulation were used to simulate the interfacial interaction between the polymers (GAP, GAP-DMH) and RDX, and the mesoscopic morphologies of GAP composite propellants. Dimethyl hydantoin grafted onto GAP is able to vary the conformations of GAP on the surfaces of RDX,

shorten the distance between GAP and RDX, and strengthen the interaction between GAP and RDX. Additionally, GAP-DMH is able to suppress agglomeration of RDX, improves the dispersibility of RDX, and enlarges the contact surface with RDX. Dimethyl hydantoin grafted onto GAP is able to effectively improve the mechanical properties of GAP/RDX propellants.

References

[1] J. Agrawal, Recent Trends in High-Energy Materials, *Prog. Energy Combust. Sci.* **1998**, *24*, 1 – 30.
[2] N. Kubota, T. Sonobe, Combustion Mechanism of Azide Polymer, *Propellants Explos. Pyrotech.* **1988**, *13*, 172 – 177.
[3] N. Mathew, R. Picu, Molecular Conformational Stability in Cyclotrimethylene Trinitramine Crystals, *J. Chem. Phys.* **2011**, *135*, 024510.
[4] Z. A. Dreger, Y. M. Gupta, High Pressure Raman Spectroscopy of Single Crystals of Hexahydro-1,3,5-trinitro-1,3,5-triazine (RDX), *J. Phys. Chem. B* **2007**, *111*, 3893–3903.
[5] J. Agrawal, S. Walley, J. Field, High-Speed Photographic Study of the Impact Response of Ammonium Dinitramide and Glycidyl Azide Polymer, *J. Propul. Power* **1997**, *13*, 463 – 470.
[6] K. Selim, S. Özkar, L. Yilmaz, Thermal Characterization of Glycidyl Azide Polymer (GAP) and GAP-Based Binders for Composite Propellants, *J. Appl. Polym. Sci.* **2000**, *77*, 538–546.
[7] Y. Sun, S. Li, The Effect of Nitrate Esters on the Thermal Decomposition Mechanism of GAP, *J. Hazard. Mater.* **2008**, *154*, 112 – 117.
[8] M. W. Beckstead, K. Puduppakkam, P. Thakre, V. Yang, Modeling of Combustion and Ignition of Solid-Propellant Ingredients, *Prog. Energy Combust. Sci.* **2007**, *33*, 497 – 551.
[9] T. Parr, D. Hanson, Cyclotetramethylene Tetranitramine/Glycidyl Azide Polymer/Butanetriol Trinitrate Propellant Flame Structure, *Combust. Flame* **2004**, *137*, 38–49.
[10] M. Niehaus, O. Greeb, Optimization of Propellant Binders–Part Two: Macroscopic Investgation of the Mechanical Properties of Polymers, *Propellants Explos. Pyrotech.* **2004**, *29*, 333–338.
[11] A. Sikder, N. Sikder, A Review of Advanced High Performance, Insensitive and Thermally Stable Energetic Materials Emerging for Military and Space Applications, *J. Hazard. Mater.* **2004**, *112*, 1 – 15.
[12] J. Sciamareli, M. F. K. Takahashi, J. M. Teixeira, K. Iha, Solid Polyurethane-Based Composite Propellant: I-Influence of the Bonding Agent, *Quim. Nova* **2002**, *25*, 107–110.
[13] J. P. Consaga, *Dimethyl Hydantoin Bonding Agents in Solid Propellants*, US Patent 4,214,928, Secretary of Navy, Washington, DC, USA, **1980**.
[14] Y. Liu, Y. Chen, L. Shi, W. Yao, Synthesis of Three Novel Laurylamine-Derived Long-Chain Alkyl Bonding Agents and Their Interactions with RDX, *Propellants Explos. Pyrotech.* **2012**, *37*, 69–76.
[15] A. I. Martinez, E. Meaurio, B. Coto, J. R. Sarasua, Molecular Dynamics Modelling for the Analysis and Prediction of Miscibility in Polylactide/Polyvinilphenol Blends, *Polymer* **2010**, *51*, 4431–4438.
[16] M. B. Sun, Characterization of the Plasticized GAP/PEG and GAP/PCL Block Copolyurethane Binder Matrices and Its Propellants, *Propellants Explos. Pyrotech.* **2008**, *33*, 131–138.
[17] M. Li, F. Li, R. Shen, X. Guo, Molecular Dynamics Study of the Structures and Properties of RDX/GAP Propellant, *J. Hazard. Mater.* **2011**, *186*, 2031–2036.
[18] J. G. Gai, H. L. Li, C. Schrauwen, G. H. Hu, Dissipative Particle Dynamics Study on the Phase Morphologies of the Ultrahigh Molecular Weight Polyethylene/Polypropylene/ Poly(ethylene glycol) Blends, *Polymer* **2009**, *50*, 336–346.
[19] C. Choi, E. Prince, The Crystal Structure of Cyclotrimethylenetrinitramine, *Acta Crystallogr., Sect. B* **1972**, *28*, 2857 – 2862.
[20] H. C. Andersen, Molecular Dynamics Simulations at Constant Pressure and/or Temperature, *J. Chem. Phys.* **1980**, *72*, 2384.
[21] S. W. Bunte, H. Sun, Molecular Modeling of Energetic Materials: the Parameterization and Validation of Nitrate Esters in the COMPASS Force Field, *J. Phys. Chem. B* **2000**, *104*, 2477–2489.
[22] W. Zhu, J. Xiao, W. Zhu, H. Xiao, Molecular Dynamics Simulations of RDX and RDX-Based Plastic-Bonded Explosives, *J. Hazard. Mater.* **2009**, *164*, 1082 – 1088.
[23] L. Qiu, W. H. Zhu, J. J. Xiao, W. Zhu, H. M. Xiao, H. Huang, Molecular Dynamics Simulations of *trans*-1,4,5,8-Tetranitro-1,4,5,8-tetraazadecalin-Based Polymer-Bonded Explosives, *J. Phys. Chem. B* **2007**, *111*, 1559–1566.
[24] Z. Luo, J. Jiang, Molecular Dynamics and Dissipative Particle Dynamics Simulations for the Miscibility of Poly(ethylene oxide)/Poly(vinyl chloride) Blends, *Polymer* **2010**, *51*, 291–299.
[25] R. D. Groot, P. B. Warren, Dissipative Particle Dynamics: Bridging the Gap Between Atomistic and Mesoscopic Simulation, *J. Chem. Phys.* **1997**, *107*, 4423.
[26] J. Huang, Y. Wang, Control of Aggregation of Nanoparticles by Double-Hydrophilic Block Copolymers: A Dissipative Particle Dynamics Study, *J. Phys. Chem. B* **2007**, *111*, 7735–7741.
[27] S. C. C. Juan, C. Hua, C. Chen, X. Sun, H. Xi, Dissipative Particle Dynamics Simulation of a Gold Nanoparticle System, *Mol. Simulat.* **2005**, *31*, 277 – 282.
[28] T. Stifter, O. Marti, B. Bhushan, Theoretical Investigation of the Distance Dependence of Capillary and van der Waals Forces in Scanning Force Microscopy, *Phys. B* **2000**, *62*, 13667.
[29] G. Perrault, R. Lavertu, J. F. Drolet, *High-Energy Explosive or Propellant Composition*, US Patent 4,289,551, Ministry of National Defense, Ottawa, Canada, **1981**.
[30] J. R. Rice, *Foundations of Solid Mechanics, in Mechanics and Materials: Fundamentals and Linkages*, John Wiley, New York, Chapter 3, **1999**, pp. 33 – 69.
[31] J. H. Weiner, *Statistical Mechanics of Elasticity*, John Wiley, New York **2002**, p. 38 – 46.

Received: December 9, 2012
Revised: May 12, 2013
Published online: November 6, 2013

